Journal of Materials Science and Engineering A 13 (7-9) (2023) 68-81
doi: 10.17265/2161-6213/2023.7-9.002

Enhancing the Activity of N/C Catalyst for Oxygen Reduction Reaction by Fluorination

Yun Wu[1], Xinyu Lu[1], Jiawei Li[1], Hengchang Lin[1], Maosen Pan[1], Gengyu Cao[1] and Yuta Nabae[2]

1. Department of Materials Science and Engineering, Guangdong University of Petrochemical Technology, Maoming 525000, China

2. Department of Materials Science and Engineering, Tokyo Institute of Technology, 2-12-1 S8-26, Ookayama, Meguro-ku, Tokyo 152-8522, Japan

Abstract: The synthesis of non-metal carbon catalysts with high catalytic activity for ORR (oxygen reduction reaction) in acidic media is a great challenge in the field of PEMFC (proton exchange membrane fuel cells). In this research, N- and F-codoped carbon catalyst with high performance was synthesized from ZIF-8 and NH_4F, which are easily prepared structure and common chemical, respectively. The as-prepared catalyst has a high surface area of 789 m^2/g and micro-porosity of ~2 nm, facilitating more active sites to the ORR and O_2 mass transfer in the diffusion of the catalyst matrix, respectively. The prepared N/C(NH_4F) catalyst exhibited an onset potential of 0.94 V (vs. RHE) and a half-wave potential of 0.65 V in 0.1 M $HClO_4$ solution. It also showed excellent durability in the cycling test of 10,000 times and a degradation shift of half-wave potential 70 mV was observed. Its diffusion-limiting current reached 5.85 mA/cm^2 next to the theoretic value of 6 mA/cm^2, suggesting that it has plenty of active sites for ORR, which could be attributed to fluorine introduction into the N/C catalyst. It proved that the introduction of fluorine into the structure of the N/C catalyst fine-tunes the Lewis basic sites of the carbon atoms adjacent to pyridinic and graphitic nitrogen species, facilitating the adsorption of oxygen molecules in the initial step of the ORR. The correlation between the N/C catalyst activity and the fluorination provides new insight into the ORR catalyst design.

Key words: ORR, Tafel slope, F-doped, synergistic effect, Lewis basicity.

1. Introduction

PEMFC (proton exchange membrane fuel cell) fed with hydrogen and oxygen, could generate electricity with the product of water with much higher efficiency than that of an engine limited by the Carnot cycle [1, 2]. It generally uses much platinum or platinum alloy as an anode catalyst layer for HOR (hydrogen oxidation reaction) and a cathode catalyst layer for ORR (oxygen reduction reaction) [3-6]. The kinetics of HOR is fast at the anode and it needs less platinum catalyst [7]. However, the ORR kinetics over the cathode is sluggish, which uses much platinum catalyst to obtain high performance of PEMFC [8]. Platinum is a kind of scarce and highly expensive metal that confines the widespread commercial usage of PEMFC in vehicles and power plants [8-10].

Much effort has been devoted to studying non-precious metal catalysts and non-metal catalysts as alternatives to Pt catalysts [11, 12]. To solve the issue mentioned above, many researchers tried to design and synthesize non-metal catalysts, (B, N, S, P, and halogen)-doped carbon substrates of graphene, carbon nanotubes, and other carbon-based materials of Ketjen Black and black pearls, exhibiting, to some degree, catalytic activity for oxygen reduction to H_2O and H_2O_2 [13-18]. In these electrocatalysts, N-doped carbon catalysts (N/C) for the ORR have been extensively investigated due to their high potential application in PEMFC.

To date, the catalyst design, mechanism, and active sites of the N/C catalyst have been clarified through

Corresponding author: Gengyu Cao, Ph.D., professor, research fields: advanced materials for energy storage and conversion.

experiments [19, 20]. In the N/C catalysts, pyridinic, graphitic, pyrrolic, and oxygen-containing nitrogen could be generally found by XPS (X-ray photoelectron spectroscopy) studies [19]. It was revealed that the electrocatalytically active performance of the ORR is mainly attributed to the content of the pyridinic and graphitic nitrogen. The pyridinic nitrogen was clarified to be more active than the graphitic nitrogen because of their different sp^2 electronic distribution. In the occupied area at the Fermi level, carbon atoms next to pyridinic N have a localized density of states suggesting that because of the potential of electron pair donation, carbon atoms may function as Lewis bases. Furthermore, pyridinic nitrogen coordinated with two carbon atoms in a six-membered ring which are located in the edge planes or defect sites should exhibit higher catalytic performance than that of graphitic nitrogen [19]. The graphitic nitrogen bonded with three carbon atoms in a graphene hexagonal ring contributes additional electrons into the big delocalized π-system. It forms three σ-bonds with three adjacent carbon atoms. Because of the different negativity between carbon and nitrogen atoms, carbon atoms could work as weak Lewis basic sites for oxygen molecule adsorption.

The Lewis basic site of carbon in an N/C catalyst could interact with an oxygen molecule which is generally known as Lewis acid [21]. Oxygen molecules are adsorbed and activated over the carbon atoms adjacent to pyridinic or graphitic nitrogen species. The oxygen molecule is further reduced to water or hydrogen peroxide by receiving electrons and protons. Herein, it is assumed that fluorine introduction in the N/C catalyst could fine-tune the adsorption of oxygen molecules corresponding to higher activity for the ORR. In the six-membered ring system of pyridinic and graphitic nitrogen species, the heteroatom of fluorine could be introduced which could connect with carbon because of its unsaturation. The electronegativity of fluorine is 3.98 Pauling units which is much larger than that of nitrogen (3.04 Pauling units). Fluorine attracts the n-π cloud from carbon resulting in the fine adsorption of oxygen [22]. Therefore, nitrogen and fluorine could synergistically adjust the electron distribution to create Lewis basic carbon sites for oxygen molecule adsorption thereby enhancing the activity of the catalysts.

In this study, nitrogen and fluorine were both introduced to carbon structure to tune the Lewis basic sites for adsorption and activation of oxygen molecules to enhance the catalysis performance. ZIF-8 structure with low cost of raw chemicals of synthesis was chosen as an N-containing carbon precursor and further pyrolyzed to N-doped carbon (N/C) at a high temperature of 800 °C. The N/C was fluoridated by NH_4F chemical at a high temperature to prepare N/C(NH_4F) material for catalysis of the ORR in acidic media with benchmark performance. The N/C(NH_4F) catalyst shows an onset potential of 0.94 V and a half-wave potential of 0.64 V while the diffusion limiting current achieves 5.86 mA/cm^2 next to the theoretical value of 6 mA/cm^2 at 1,600 rpm. The catalytic performance is much higher than those of the counterparts of the N/C, N/C(NH_4Cl), and F/C catalysts. It proved that the introduction of fluorine into the structure of the N/C catalyst fine-tunes the Lewis basic sites of the carbon atoms adjacent to pyridinic and graphitic nitrogen species, facilitating the adsorption of oxygen molecules in the initial step of the ORR.

2. Experimental

2.1 Synthesis of ZIF-8 Material

Typically, 2.94 g of $Zn(NO_3)_2 \cdot 6H_2O$ was dissolved in 100 mL methanol. Then 3.24 g of 2-methylimidazole was dissolved similarly in 100 mL of methanol [11]. Two kinds of solution were quickly mixed and then stirred for 0.5 h. The white precipitate was separated by centrifugation at 10,000 rpm, washed three times, and finally dried at 60 °C overnight.

2.2 Synthesis of N/C and N/C(NH_4F) Catalysts

The synthesized ZIF-8 powder was pyrolyzed at

800 °C for 3 h in a nitrogen atmosphere to prepare the N/C catalyst. The as-prepared N/C powder was dispersed in 10 mL water containing NH_4F in which the mass ratio between N/C power and NH_4F was 1:1. The mixture was sonicated for 30 min and then stirred overnight. Finally, the resulting suspension was dried at 60 °C. The obtained powder was pyrolyzed at 1,000 °C for 1 h under nitrogen flow to obtain an N/C(NH_4F) catalyst which was elucidated in Fig. 1. N/C(NH_4Cl) catalyst was prepared in the same way where the NH_4F was substituted by NH_4Cl. For comparison, the F/C catalyst was prepared from Ketjen Black and NH_4F with a mass ratio of 1:1 at 1,000 °C for 1 h under nitrogen.

2.3 Characterization

The morphology of the materials was characterized through Field-emission-scanning electron microscopy (FE-SEM; Hitachi Regulus 8220). Diffraction data for XRD spectra were collected from 10° to 90° in a step of 0.01° (Rigaku, Ultima IV). The Raman spectroscopy was performed using a Thermo Scientific DXR2 Raman microscope with a laser source of 532 nm. TEM (transmission electron microscopy) images were obtained using a Thermo Fisher Talos F200X at 200 kV. XPS analysis was performed using an ESCALAB Xi+ spectrometer (Thermo Fischer) equipped with a monochromator and an Al anode at 12.5 kV and 16 mA. To compensate for electrostatic charge, the XPS spectra were corrected to the internal reference spectra of C 1s at 284.5 eV, which is the binding energy of the C=C bond of catalysts. The binding energies of different elements were referred to the NIST XPS Database.

2.4 Electrochemical Characterization

All of the electrochemical measurements were performed using a Solartron 1470E with the system of RRDE (Rotating Ring Disk Electrode) of ALS (Japan). The RRDE was composed of a 4 mm diameter glassy disk (0.1256 cm^2) and Pt ring (0.1885 cm^2). Carbon fiber connected with the carbon rod was used as the counter electrode while Ag/AgCl (sat. KCl) was used as the reference electrode. The potential was corrected to a RHE (reversible hydrogen electrode). The modified electrode was rinsed with 0.1 M $HClO_4$ solution to avoid air-droplet formation on the electrode surface before measurement. The rotation speed of the RRDE was 1,600 rpm. The disk potential was scanned from 0 to 1.1 V while the ring potential was held at 1.2 V. On the basis of the measured data, the electron transfer number and hydrogen peroxide fraction were determined by the following equations.

$$n = \frac{4I_D}{I_D + \frac{I_R}{N}} \quad (1)$$

$$H_2O_2\% = \frac{200 * \frac{I_R}{N}}{I_D + \frac{I_R}{N}} \quad (2)$$

Here, I_D and I_R are the disk current and ring current, respectively. N is the collection efficiency measured in a 0.1 M $HClO_4$ solution containing 2 mM $FeCl_3$.

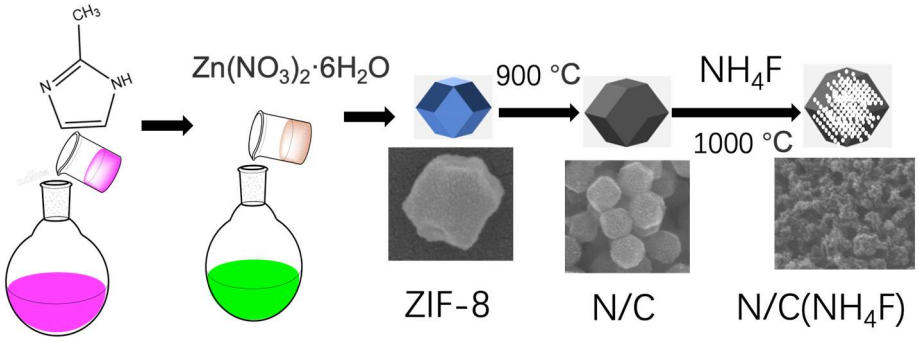

Fig. 1 A schematic synthesis process of the N/C(NH_4F) catalyst.

2.5 Preparation of Modified Electrode

Five milligrams of catalyst power were exactly weighed into a 2 mL vial, and dispersed in the mixture of 150 μL of ethanol, 150 μL of Milli Q-water (18.2 MΩ), and 50 μL of 5 wt % Nafion. The obtained suspension was sonicated in water with ice for 30 min to prepare uniform ink. Seven microliters of catalyst ink were pipetted onto the glassy carbon disc electrode surface of the RRDE (rotating ring disc electrode) which was polished and washed before usage. The electrode was dried under nitrogen flow. Finally, the catalyst loading was calculated to be 795 μg/cm^2.

3. Results and Discussion

The N/C catalyst with a nano-size of 100 nm in Fig. 2a shows the framework structure of the dodecahedron prepared from pyrolysis of ZIF-8 at 800 °C in a nitrogen atmosphere. The N/C(NH_4F) catalyst in Fig. 2b shows a much smaller particle size compared with its counterpart of the N/C catalyst. It suggests that the framework structure was lost in the fluorination condition of NH_4F at a high temperature of 1,000 °C. XRD spectroscopy of the N/C catalyst in Fig. 2c shows two peaks at 24.8° (002) and 43.9° (100), whose intensities are lower than that of the N/C(NH_4F) catalyst. It illustrates that the graphitization of the N/C(NH_4F) catalyst is higher than that of the N/C catalyst. The FWHM (full width at half maximum) of the (100) and (002) peaks of the N/C(NH_4F) catalyst corresponds to a larger size of L_a and L_c of the carbon structure [23, 24]. The (002) Bragg peak for the N/C(NH_4F) catalyst is smaller than that of the N/C catalyst corresponding to the fact that the spacing between the graphene layers slightly increases after the introduction of fluorine. I_D/I_G ratio of the N/C(NH_4F) catalyst displayed in Fig. 2d is much higher than that of the N/C catalyst suggesting that the fluorination process creates defective sites. Fig. 2e displays the N/C(NH_4F) catalyst (789 m^2/g) has a higher surface area than that of the N/C (541 m^2/g). However, the N/C(NH_4F) catalyst has a much smaller surface area than that of the N/C(NH_4Cl) (1,025 m^2/g). Fig. 2f illustrates that the N/C(NH_4F) and N/C(NH_4Cl) catalysts have micropores due to ammonia etching at high temperatures.

The microstructure of the N/C(NH_4F) catalyst was shown in Fig. 3. The nanoparticles aggregated together to form pores for oxygen molecule diffusion. The shape of the nanoparticles was not uniform. The high-resolution TEM image in Fig. 3b shows that the carbon was an amorphous structure similar to the stacking onion planes. The selected area electron diffraction pattern in Fig. 3c further verifies the amorphous structure of the N/C(NH_4F) catalyst. The large degree of the amorphous structure corresponds to more defect sites for catalysis. The mapping images of the N/C(NH_4F) catalyst (Figs. 3d-3f) show that the catalyst contains the elements of C, N, F, O, and Zn. N and F elements are uniformly distributed in the catalyst.

The survey scan of the N/C catalyst in Fig. 4a proves the existence of C, N, O, and Zn elements. The sharp peak of C 1s at 284.5 eV (olive) is ascribed to sp2 carbon with C=C bonds. The peak at 285.8 eV (purple) is ascribed to the C=N bond while the peak of 288.5 eV (dark yellow) corresponds to oxygen-containing carbon. The carbon accounts for 79.37 atomic% shown in Table 1. N1s in Fig. 4c is ascribed to pyridinic-N at 398.0 eV (olive), pyrrolic-N at 400.4 eV (purple), and graphitic-N at 398.9 eV (dark yellow). It is worth noting that the N/C catalyst was N-rich species accounting for 8.89 atomic% (Table 1). Zn2p peak in Fig. 4d reveals the N/C catalyst contains Zn element (1.14%). The peaks located at 1,044.4 and 1,021.4 eV correspond to $Zn2p_{1/2}$ and $Zn2p_{3/2}$, respectively.

The survey scan of the N/C(NH_4F) catalyst in Fig. 5a confirms that it contains the elements of C, N, O, and Zn. The peak information for fluorine is not clear. After fluorine doping, a new fitting peak at 285.2 eV (dark cyan) ascribed to the C-F bond is observed in Fig. 5b. The peak for the C-N bond shifts from 285.8 to 286.3 eV while the peak for O-

containing carbon species shifts from 288.5 to 288.7 eV. The fitting peak for pyridinic-N shifts from 398.0 to 398.4 eV while graphitic-N shifts from 398.9 to 399.5 eV in Fig. 5c. The peak intensity for Zn in Fig. 6d decreased from 1.14 atomic% to 0.15 atomic% shown in Table 1.

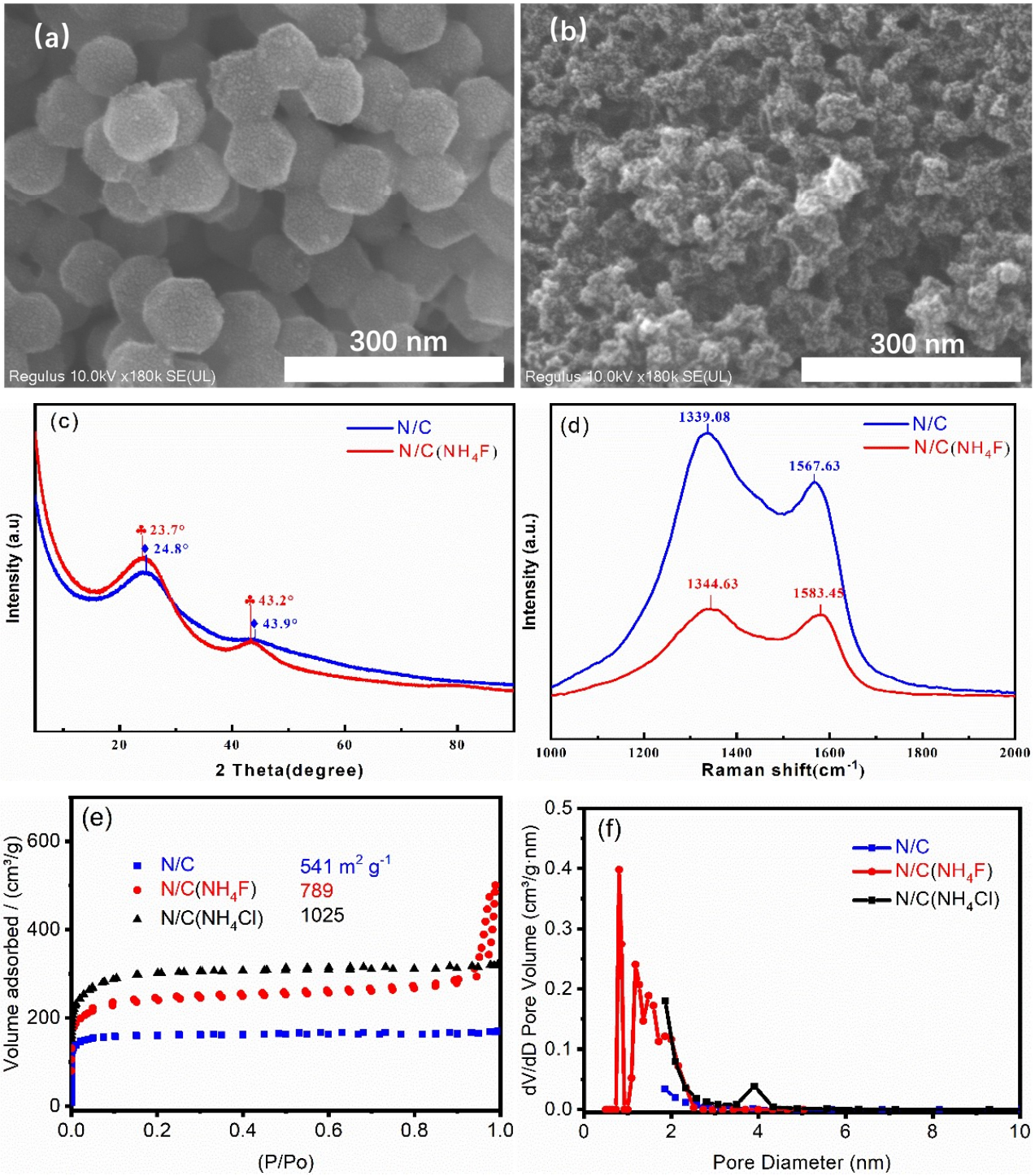

Fig. 2 SEM images of the N/C (a) and the N/C(NH_4F) (b) catalysts. (c) XRD patterns of the N/C and N/C(NH_4F) catalyst powders. (d) Raman spectra of the N/C and the N/C(NH_4F) catalyst. (e) N_2 sorption isotherms. (d) Pore size distributions of the catalysts. *dV*/*dD*, differential pore volume distribution; *V*, pore volume; *D*, pore diameter.

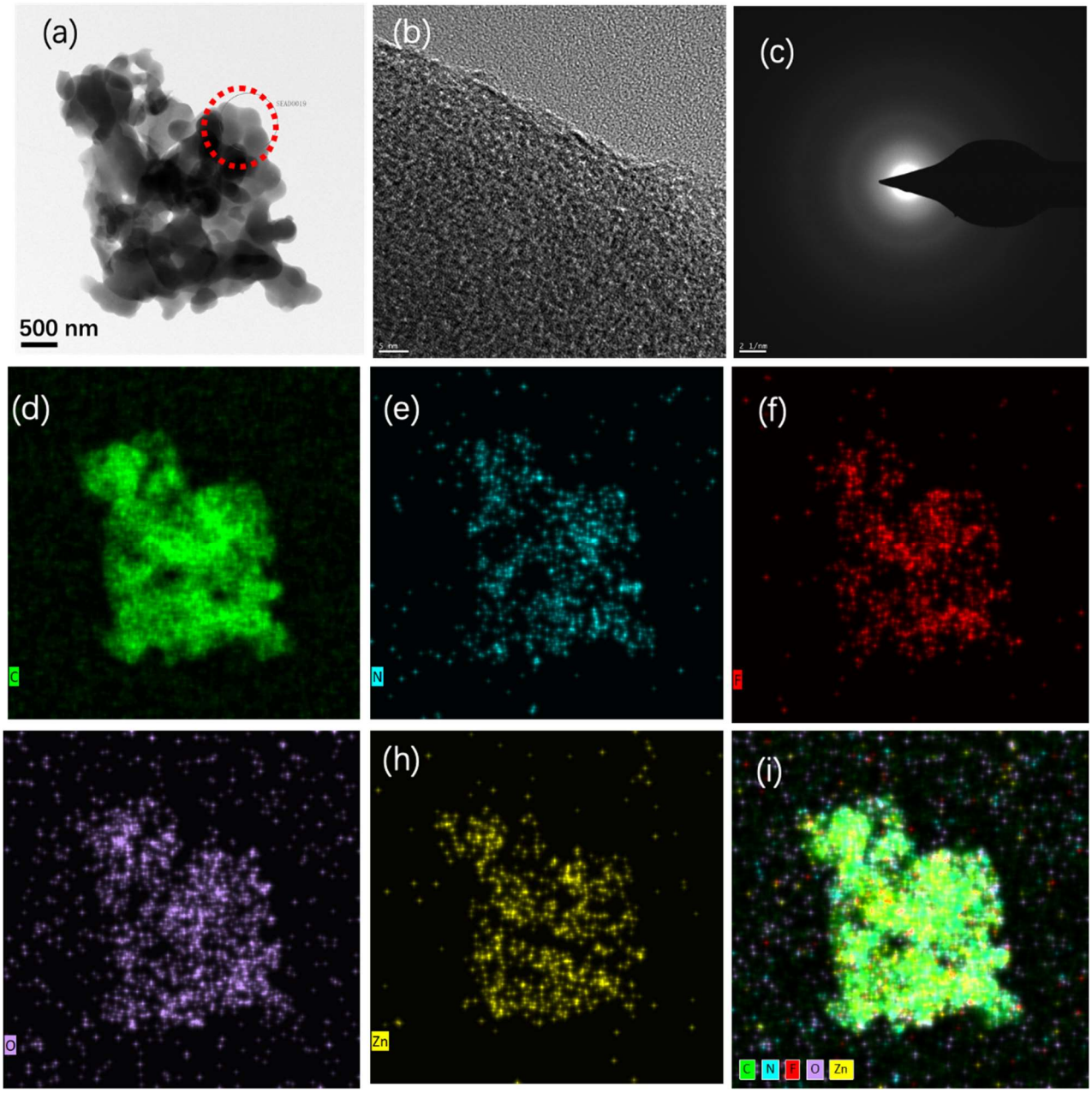

Fig. 3 (a) TEM images for the as-prepared N/C(NH_4) catalyst. (b) high-resolution TEM images for the selected area. (c) Electron diffraction pattern of the N/C(NH_4F) catalyst (selected area). (d)-(h) Elemental mapping of C, N, F, O, and Zn. (i) Mixed elemental mapping image.

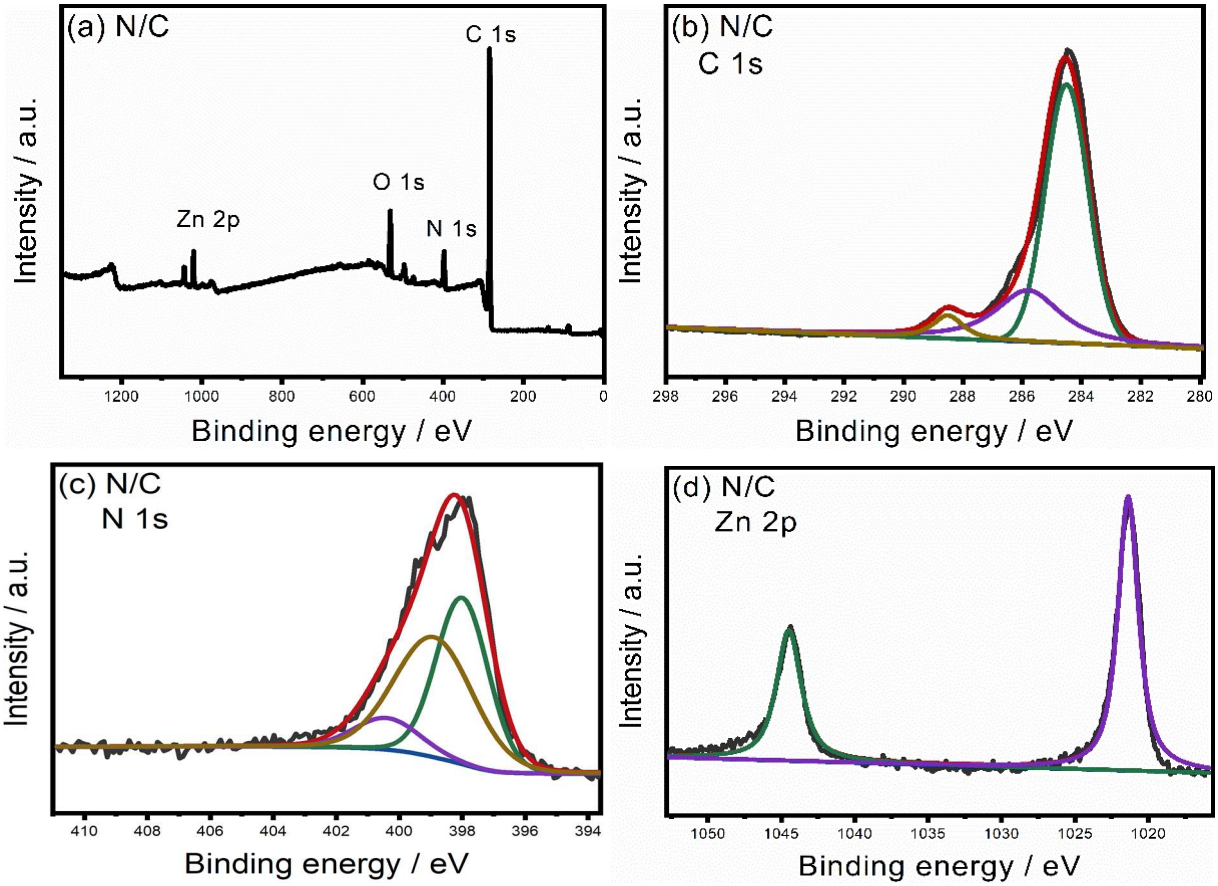

Fig. 4 XPS characterization of the N/C catalyst. (a) Survey scan of the N/C catalyst. (b)-(d) High-resolution spectra of C1s, N1s, and Zn2p.

Table 1 Atomic content of different elements in the N/C and N/C(NH_4F) catalysts..

Element	Atomic% of N/C	Atomic% of N/C(NH_4F)
C	79.73	83.42
N	8.89	3.85
F	/	0.44
O	9.96	12.14
Zn	1.14	0.15

The peak at 648.5 eV illustrated in Fig. 5e is ascribed to fluorine which accounts for 0.44 atomic % in the N/C(NH_4F) catalyst. The above-mentioned analysis of the binding energy of different species suggests that the F-doping makes an effect on the cloud of carbon and nitrogen in the catalyst. F atoms in the structure attract the electron cloud of carbon and nitrogen atoms, leading to electronic distribution in a new way.

In order to compare the ORR electrocatalytic activities of the N/C and the N/C(NH_4F) catalysts, RRDE voltammograms were performed. The N/C catalyst displayed in Fig. 6a shows an onset potential ($E_{on\text{-}set}$) of 0.801 V and a half-wave potential ($E_{1/2}$) of 0.38 V comparable to the other kinds of N-doped carbon catalysts. Its apparent electron transfer number is approximately 3 between 0 and 0.8 V while the hydrogen peroxide yield approached 60%, suggesting that the N/C catalyst pyrolyzed from ZIF-8 for ORR in this study is the 2-e predominant process. After fluorine introduction, the N/C(NH_4F) shows much higher activity. The onset potential and the half-wave potential are 0.94 (at 30 μA/cm^2) and 0.65 V, respectively. The diffusion-limiting current density reached almost 5.86 mA/cm^2 which is next to the theoretical current density of the RDE at 1,600 rpm (6 mA/cm^2). The ORR activity of the N/C(NH_4F) catalyst is completely controlled by the mass transfer of oxygen in the limiting diffusion potential range between 0 and 0.4 V. It suggests that the

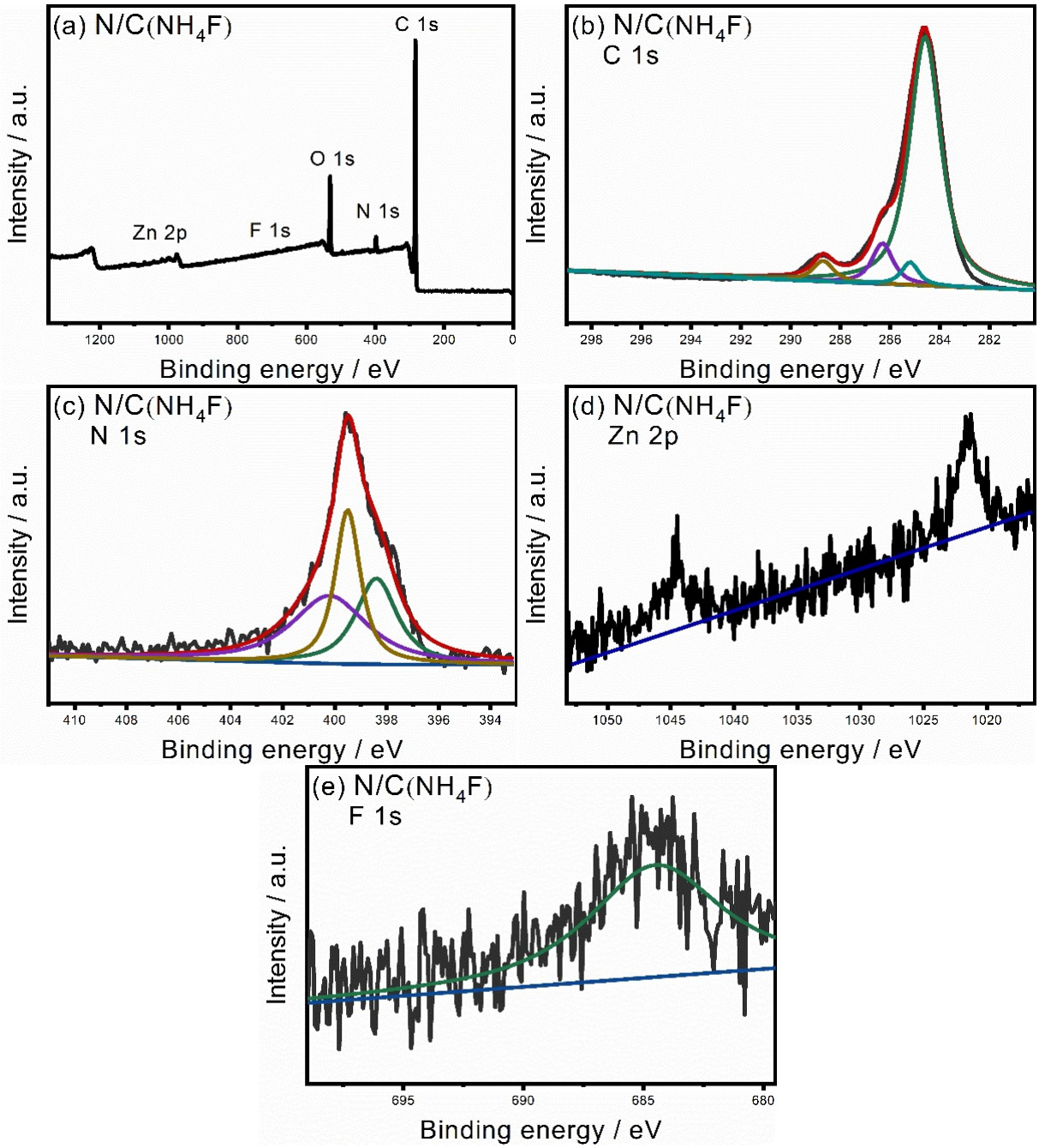

Fig. 5 XPS characterization of N/C(NH_4F) catalyst. (a) Survey scan of the N/C(NH_4F) catalyst. (b)-(e) High-resolution spectra of C1s, N1s, Zn2p, and F1s.

N/C(NH_4F) catalyst has enough active sites for oxygen adsorption. It is interesting that the N/C in Fig. 6b shows a lower hydrogen peroxide yield at a higher potential kinetic range between 0.5 and 0.8 V than that between 0 and 0.5 V. However, the N/C(NH_4F) shows a sharp contrast tendency compared with the N/C catalyst, which is consistent with the transparent electron number. It reveals that after fluorine introduction, the electrocatalytic activity was greatly enhanced. The N/C(NH_4Cl) catalyst exhibits slightly lower activity compared with that of the N/C(NH_4F) even though the N/C(NH_4Cl) has a much higher surface area (23% more than that of the N/C(NH_4F)). Generally, a high surface area of the catalyst corresponds to a high

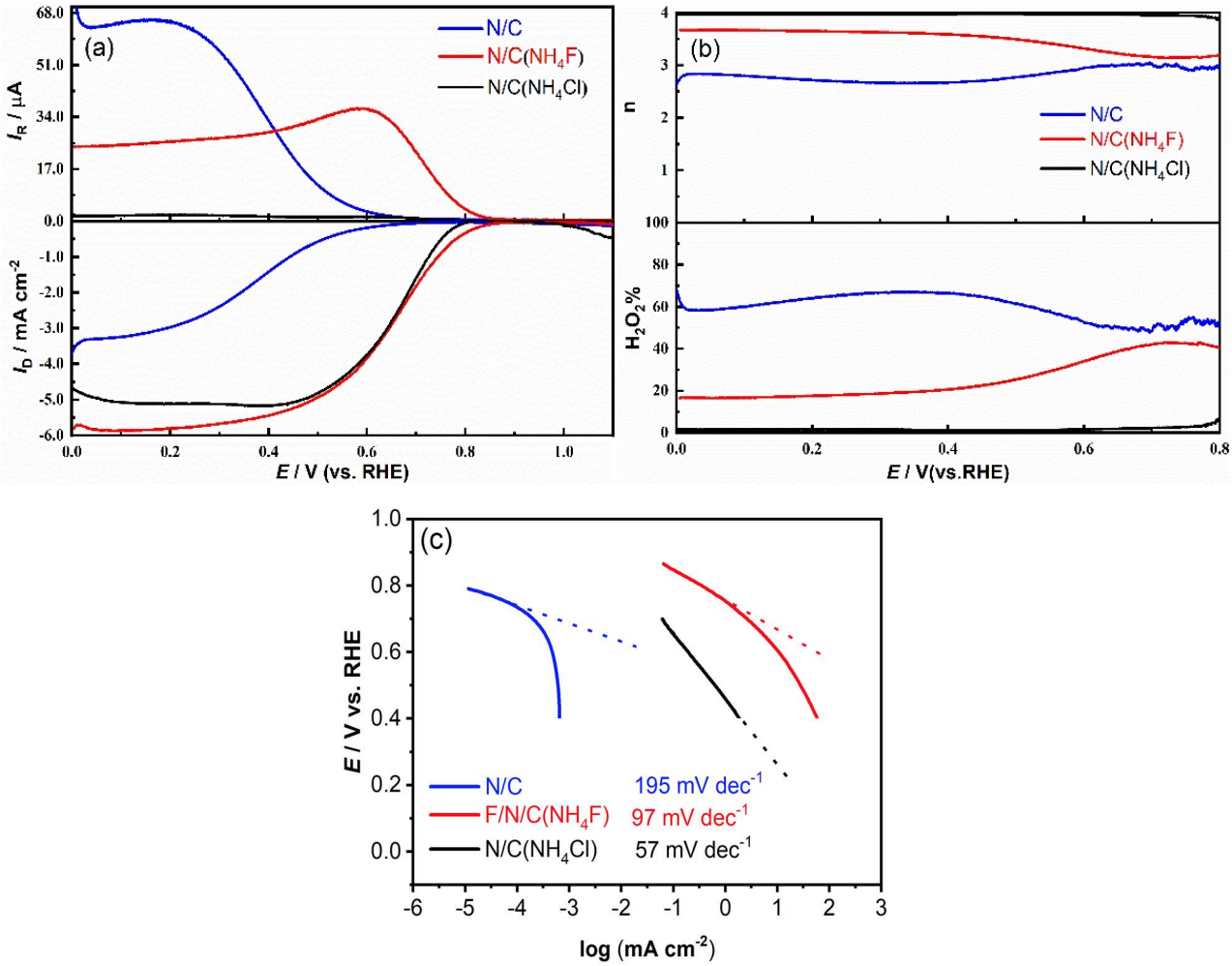

Fig. 6 Comparison of electrochemical performance for the N/C, N/C(NH_4F) and N/C(NH_4Cl) catalysts. (a) RRDE voltammograms for the ORR of the N/C (blue), N/C(NH_4F) (red), and N/C(NH_4Cl) (black) catalysts in O_2-saturated 0.1 M $HClO_4$ solution. (b) Calculated electron transfer number and percentage of hydrogen peroxide produced over the catalysts. (c) Tafel plots for the catalysts. Electrode rotation speed: 1,600 rpm. Scan rate: 10 mV/s. loading density: 795 μg/cm^2.

catalytic current for the ORR because of the more active sites exposed. Herein, it is inferred that the high activity of the N/C(NH_4F) is attributed to the fluorine doping but not the high surface area caused by ammonia etching. It is observed that the NH_4Cl could create a higher surface area and more porosity for the N/C catalyst at a high temperature than that of the NH_4F agent resulting in a lower H_2O_2 yield.

It was reported that pyridinic and graphitic nitrogen species contribute to the activity of the N/C catalyst [25]. Pyridinic and graphitic nitrogen species create Lewis basic sites for the ORR. The ORR active sites in the N/C catalyst are carbon atoms with Lewis basicity adjacent to pyridinic and graphitic nitrogen atoms. The active site created by the pyridinic nitrogen atom has higher activity for the ORR than that of graphitic nitrogen atoms because the active site adjacent to the pyridinic atom possesses stronger adsorption for the O_2 molecule than that of the graphitic nitrogen atom. After the introduction of the fluorine element, the Lewis basic sites created by the pyridinic and the graphitic nitrogen species are fine-tuned if the fluorine is added to the unsaturated carbon in the six-membered ring with a nitrogen atom. The co-doping of N and F of the carbon correlates to a higher activity of the ORR than that of N-doped carbon.

The N/C catalyst exhibits a Tafel slope of -195 mV/dec in Fig. 6c suggesting that the non-electron-transferring step is the RDS (rate-determining step). The N/C(NH_4F) catalyst shows a Tafel slope of -97 mV/dec at a high potential range, suggesting a mixed process armed with a one-electron transfer step and two-electron transfer in the RDS [26]. The N/C(NH_4F) catalyzes ORR in acidic media through different methods depending on active sites. As is known, Pt catalysts reduce oxygen molecules with a dissociation mechanism at a high potential range corresponding to 2e transferring in RDS with a Tafel slope of -60 mV/dec while it has an association mechanism at a lower potential range corresponding to one-electron transferring in RDS with -120 mV/dec [27].

Some active sites of the N/C(NH_4F) catalyst facilitate the ORR process with one electron transfer in a rate-determined step, corresponding to the possible mechanism of association [27] as follows:

$$* + O_2 \rightarrow *O_2 \quad (3)$$

$$*O_2 + H^+ + e^- \rightarrow *OOH \quad (4)$$

$$*OOH + H^+ + e^- \rightarrow *O + H_2O \quad (5)$$

$$*O + H^+ + e^- \rightarrow *OH \quad (6)$$

$$*OH + H^+ + e^- \rightarrow * + H_2O \quad (7)$$

where * is adsorbing sites over the catalyst. Firstly, the oxygen molecule in the solution is adsorbed end-on on active sites shown in Eq. (3) [27, 28]. It was reduced to the intermediate of OOH via a proton and an electron in Eq. (4) [22]. This is the RDS for the ORR corresponding to the theoretical Tafel slope of -120 mV/dec in the RDE voltammetry. Therefore, the above-mentioned mechanism is proved. Part of oxygen is reduced to hydrogen peroxide and further reduced to water. The corresponding mechanism is described as follows:

$$*OOH + H^+ + e^- \rightarrow * + H_2O_2 \quad (6)$$

$$*H_2O_2 + 2H^+ + 2e^- \rightarrow * + 2H_2O \quad (7)$$

Some active sites of the N/C(NH_4F) catalyst facilitate the ORR process with 2e predominant transfer in the RDS, corresponding to the possible mechanism of dissociation [27] as follows:

$$2* + O_2 \rightarrow 2*O \quad (8)$$

$$2*O + 2H^+ + 2e^- \rightarrow 2*OH \quad (9)$$

$$2*OH + 2H^+ + 2e^- \rightarrow 2* + 2H_2O \quad (10)$$

2* stands for bridge sites for oxygen molecule adsorption sites [27]. The formation of 2*OH is the RDS, corresponding to the theoretic Tafel slope of -60 mV/dec. It is convinced that there are different active sites with different activation processes over the N/C(NH_4F) catalyst. The active sites with dissociation mechanism over the N/C(NH_4F) may be attributed to the high surface area and micropores created by ammonia from NH_4F at high temperatures, which was proved by the ORR process of the N/C(NH_4Cl) with -60 mV/dec.

To clarify the synergistic effects of F and N dopants in the structure of the N/C(NH_4F) catalyst, the F/C catalyst was synthesized from Ketjen Black and NH_4F with a mass ratio of 1:1 at 1,000 °C similar to that of the N/C(NH_4F) catalyst. The F/C catalyst in Fig. 7a catalyzes ORR with an onset potential and half-wave potential of 0.74 V and 0.43 V, respectively. The pathway of ORR is a 2e predominant process and its H_2O_2 yield approached 70%-90%. The catalytic performance is similar to that of the N/C catalyst. The active sites of both the N/C and the F/C catalysts were much lower than that of the N/C(NH_4F) catalyst, suggesting the synergistic effects of F and N dopants in tailoring the electronic arrangement of the catalysts. As displayed in Fig. 8, there are two kinds of N species creating active sites for the ORR, pyridinic, and graphitic nitrogen. F atoms could exist on the edges, the planes, or the defect sites of the graphene in the form of covalent, ionic, and semi-ionic bonds [29]. It means that the F atom could bind with any carbon atom in the N/C catalyst structure. Both the N and the F atoms in the catalyst tune the electron distribution to create Lewis basic sites for the ORR with proper activation energy.

Fig. 9 shows the durability test for the N/C(NH_4F) catalyst. The ring current in Fig. 9a for hydrogen peroxide collection slightly increases with the potential cycling number. After cycling 10,000 times between

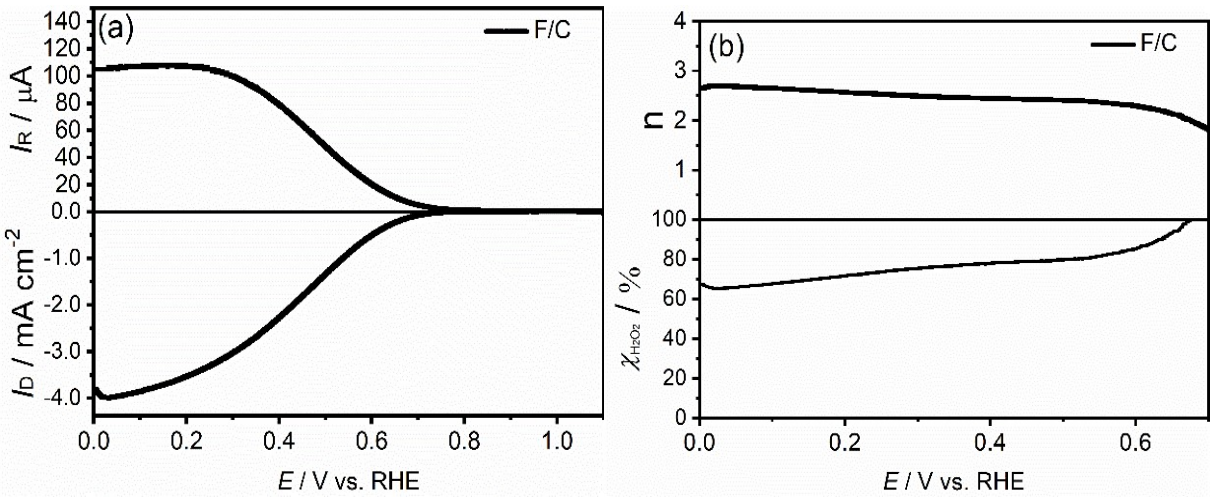

Fig. 7 (a) RRDE voltammograms for the ORR of the F/C catalyst in O_2-saturated 0.1 M $HClO_4$ solution. (b) Calculated electron transfer number and percentage of hydrogen peroxide produced over the F/C catalyst. Electrode rotation speed: 1,600 rpm. Scan rate: 10 mV/s. Loading density: 795 μg/cm^2.

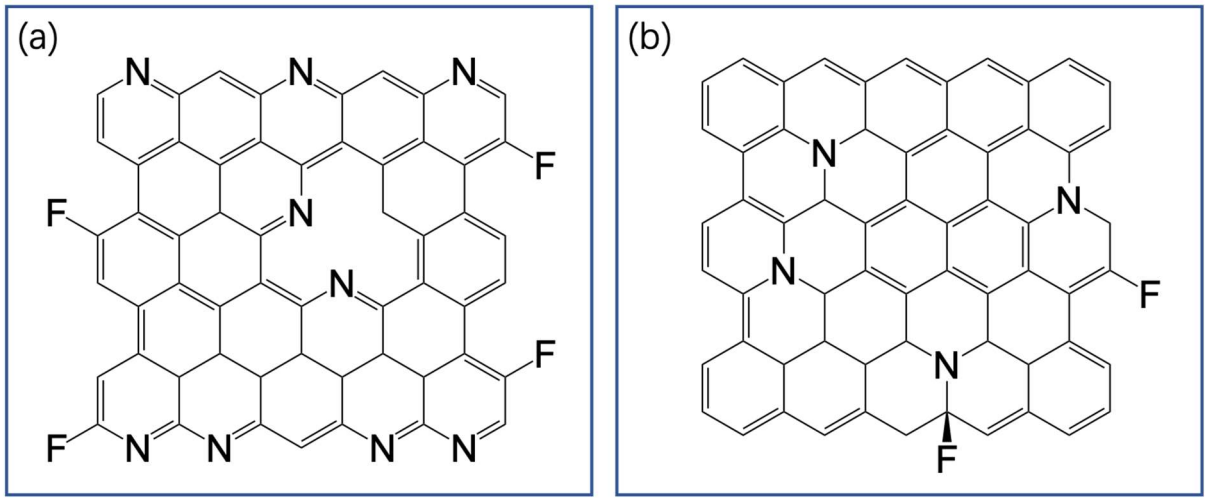

Fig. 8 Schematic for different nitrogen species and the corresponding fluorine atom in the same ring. (a) Fluorine atoms tune the activity of Lewis basic sites created by Pyridinic nitrogen species. (b) Fluorine atoms tune the activity of Lewis basic sites created by graphitic nitrogen species.

0.6 and 1 V at 0.5 V/s. As displayed in Fig. 9b-9d, the onset potential of the N/C(NH_4F) catalyst degraded from 0.94 V to 0.89 V, while the half-wave potential shifted from 0.65 to 0.58 V (70 mV). The diffusion limiting current density varied from 5.86 to 5.56 mA/cm^2, suggesting that the active sites for the ORR are very stable. The potential cycling measurement demonstrates that the catalyst is quite durable in catalyzing ORR. The existence of the C-F bonds with stronger bond energy in the catalyst was credited with exceptional durability [30]. Compared with other F-containing catalysts for the ORR in acidic media displayed in Table 2, the N/C(NH_4F) catalyst in this study shows high activity.

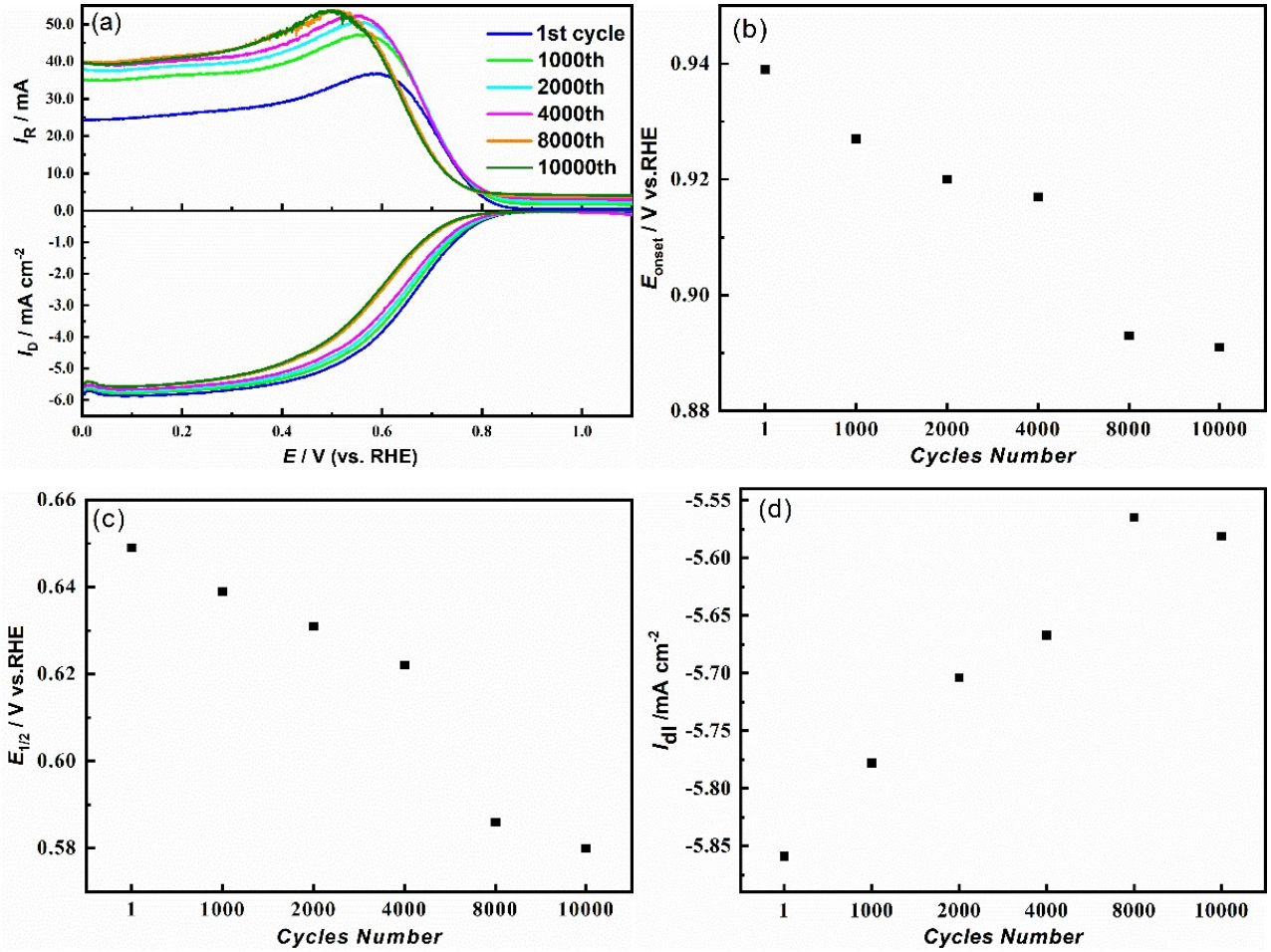

Fig. 9 Durability test for the N/C(NH4F) catalyst. (a) RRDE polarization curves of the N/C(NH4F) catalyst before and after potential cycling in O2-saturated 0.1 M HClO4. Potential cycling was carried out between 0.6 and 1.0 V versus RHE at 500 mV/s. (b) E_{onset} shift with the number of potential cycles. (c) $E_{1/2}$ shift with the number of potential cycles. (d) I_{dl} shift with the number of potential cycles.

Table 2 ORR performance of fluorine and nitrogen co-doped carbon catalysts obtained from RRDE in acidic media.

Catalyst	E_{onset}	$E_{1/2}$	Media	Ref.
N/C(NH4F)	0.94	0.65	$HClO_4$	This study
F/C	0.90	0.63	H_2SO_4	[13]
C-Mela-PTFE	0.90	0.64	$HClO_4$	[31]
N-F/GNF	0.90	0.63	$HClO_4$	[32]

4. Conclusions

In order to clarify the effect of fluorine introduction into the N/C catalyst posed to the activity of the ORR, a N/C(NH4F) catalyst has been developed through fluorination of N-doped carbon pyrolyzed from ZIF-8. The N/C(NH4F) catalyst shows high activity for ORR in acidic media with an onset potential of 0.94 V (vs. RHE) and a half-wave potential of 0.65 V. The N/C(NH4F) exhibits higher activity than that of its counterparts of the N/C, N/C(NH4Cl), and F/C catalysts, which is attributed to the synergistic effect of N and F in the catalyst. A shift of 70 mV of half-wave potential after cyclic scans of 10,000 times was observed, verifying the remarkable durability of the catalyst due to the C-F bond with strong binding energy. This study found that F- and N-codoping could enhance the catalytic activity of carbon catalysts for the ORR in

acidic media by tailoring the electronic distribution of the structure. It proved fluorine introduction in the N/C catalyst could fine-tune the adsorption of oxygen molecules corresponding to higher activity for the ORR.

Acknowledgments

This work was financially supported by Projects of Talents Recruitment and PhDs' Start-up Research of GDUPT, Guangdong Province Science and Technology Innovation Strategic Project (2023S005049), Guangdong Basic and Applied Basic Research Foundation (2022A1515011927), and Characteristic Innovation Foundation of Guangdong Province (2020KTSCX082).

Author Contributions

X.L. prepared the catalysts and conducted the electrochemical measurements. J.L. measured the durability of the catalyst and made the figures. Y.W. designed the research and wrote the manuscript. G.C. and Y.N. revised the manuscript and joined the discussion of the manuscript.

Conflict of Interests

The authors declare no competing interests.

References

[1] Dusastre, V. 2010. *Materials for Sustainable Energy: A Collection of Peer-Reviewed Research and Review Articles from Nature Publishing Group*. Hackensack: World Scientific.

[2] Yeager, E. 1961. "Fuel Cells: They Produce More Electricity per Pound of Fuel than Any Other Nonnuclear Method of Power Production." *Science* 134: 1178-86. https://doi.org/10.1126/science.134.3486.1178.

[3] Bu, L., Zhang, N., Guo, S., Zhang, X., Li, J., Yao, J., Wu, T., Lu, G., Ma, J.-Y., Su, D., and Huang, X. 2016. "Biaxially Strained PtPb/Pt Core/Shell Nanoplate Boosts Oxygen Reduction Catalysis." *Science* 354: 1410-4. https://doi.org/10.1126/science.aah6133.

[4] Li, M., Zhao, Z., Cheng, T., Fortunelli, A., Chen, C.-Y., Yu, R., Zhang, Q., Gu, L., Merinov, B. V., Lin, Z., Zhu, E., Yu, T., Jia, Q., Guo, J., Zhang, L., Goddard, W. A., Huang, Y., and Duan, X. 2016. "Ultrafine Jagged Platinum Nanowires Enable Ultrahigh Mass Activity for the Oxygen Reduction Reaction." *Science* 354: 1414-9. https://doi.org/10.1126/science.aaf9050.

[5] Escudero-Escribano, M., Malacrida, P., Hansen, M. H., Vej-Hansen, U. G., Velazquez-Palenzuela, A., Tripkovic, V., Schiotz, J., Rossmeisl, J., Stephens, I. E. L., and Chorkendorff, I. 2016. "Tuning the Activity of Pt Alloy Electrocatalysts by Means of the Lanthanide Contraction." *Science* 352: 73-6. https://doi.org/10.1126/science.aad8892.

[6] Chong, L., Wen, J., Kubal, J., Sen, F. G., Zou, J., Greeley, J., Chan, M., Barkholtz, H., Ding, W., and Liu, D.-J. 2018. "Ultralow-Loading Platinum-Cobalt Fuel Cell Catalysts Derived from Imidazolate Frameworks." *Science* 362: 1276-81. https://doi.org/10.1126/science.aau0630.

[7] Sheng, W., Gasteiger, H. A., and Shao-Horn, Y. 2010. "Hydrogen Oxidation and Evolution Reaction Kinetics on Platinum: Acid vs. Alkaline Electrolytes." *J. Electrochem. Soc*. 157: B1529. https://doi.org/10.1149/1.3483106.

[8] Wu, Y., and Nabae, Y. 2021. "Rotating Ring-Disk Electrode Theory and Method to Correct Quasi-Four-Electron Oxygen Reduction over Fe/N/C and N/C Cathode Catalysts." *Curr. Opin. Electrochem*. 25: 100633. https://doi.org/10.1016/j.coelec.2020.08.015.

[9] Wan, X., Liu, X., Li, Y., Yu, R., Zheng, L., Yan, W., Wang, H., Xu, M., and Shui, J. 2019. "Fe-N-C Electrocatalyst with Dense Active Sites and Efficient Mass Transport for High-Performance Proton Exchange Membrane Fuel Cells." *Nat. Catal.* 2: 259-68. https://doi.org/10.1038/s41929-019-0237-3.

[10] Li, J., Chen, M., Cullen, D. A., Hwang, S., Wang, M., Li, B., Liu, K., Karakalos, S., Lucero, M., Zhang, H., Lei, C., Xu, H., Sterbinsky, G. E., Feng, Z., Su, D., More, K. L., Wang, G., Wang, Z., and Wu, G. 2018. "Atomically Dispersed Manganese Catalysts for Oxygen Reduction in Proton-Exchange Membrane Fuel Cells." *Nat. Catal*. 1: 935-45. https://doi.org/10.1038/s41929-018-0164-8.

[11] Li, Y., Zhou, W., Wang, H., Xie, L., Liang, Y., Wei, F., Idrobo, J.-C., Pennycook, S. J., and Dai, H. 2012. "An Oxygen Reduction Electrocatalyst Based on Carbon Nanotube-Graphene Complexes." *Nat. Nanotechnol.* 7: 394-400. https://doi.org/10.1038/nnano.2012.72.

[12] Muthukrishnan, A., Nabae, Y., Okajima, T., and Ohsaka, T. 2015. "A Kinetic Approach to Investigate the Mechanistic Pathways of Oxygen Reduction Reaction on Fe- Containing N-Doped Carbon Catalysts." *ACS Catal.* 9 (5): 5194-202.

[13] Sun, X., Song, P., Liu, J., and Xu, W. 2013. "Fluorine-Doped BP 2000: Highly Efficient Metal-Free Electrocatalysts for Acidic Oxygen Reduction Reaction with Superlow H_2O_2 Yield." *Chem. Commun.* 49: 10296. https://doi.org/10.1039/c3cc45480k.

[14] Wu, Y., Muthukrishnan, A., Nagata, S., and Nabae, Y. 2019. "Kinetic Understanding of the Reduction of Oxygen to Hydrogen Peroxide over an N-Doped Carbon

Electrocatalyst." *J. Phys. Chem. C* 123: 4590-6. https://doi.org/10.1021/acs.jpcc.8b12464.

[15] Dai, L., Xue, Y., Qu, L., Choi, H.-J., and Baek, J.-B. 2015. "Metal-Free Catalysts for Oxygen Reduction Reaction." *Chem. Rev.* 115: 4823-92. https://doi.org/10.1021/cr5003563.

[16] Liu, X., and Dai, L. 2016. "Carbon-Based Metal-Free Catalysts." *Nat. Rev. Mater.* 1: 16064. https://doi.org/10.1038/natrevmats.2016.64.

[17] Choi, C. H., Park, S. H., and Woo, S. I. 2012. "Binary and Ternary Doping of Nitrogen, Boron, and Phosphorus into Carbon for Enhancing Electrochemical Oxygen Reduction Activity." *ACS Nano*. 6: 7084-91. https://doi.org/10.1021/nn3021234.

[18] Ishizaki, T., Wada, Y., Chiba, S., Kumagai, S., Lee, H., Serizawa, A., Li, O. L., and Panomsuwan, G. 2016. "Effects of Halogen Doping on Nanocarbon Catalysts Synthesized by a Solution Plasma Process for the Oxygen Reduction Reaction." *Phys. Chem. Chem. Phys*. 18: 21843-51. https://doi.org/10.1039/C6CP03579E.

[19] Deng, H., Li, Q., Liu, J., and Wang, F. 2017. "Active Sites for Oxygen Reduction Reaction on Nitrogen-Doped Carbon Nanotubes Derived from Polyaniline." *Carbon* 112: 219-29. https://doi.org/10.1016/j.carbon.2016.11.014.

[20] Guo, D., Shibuya, R., Akiba, C., Saji, S., Kondo, T., and Nakamura, J. 2016. "Active Sites of Nitrogen-Doped Carbon Materials for Oxygen Reduction Reaction Clarified Using Model Catalysts." *Science* 351: 361-5. https://doi.org/10.1126/science.aad0832.

[21] Guo, D., Shibuya, R., Akiba, C., Saji, S., Kondo, T., and Nakamura, J. 2016. "Active Sites of Nitrogen-Doped Carbon Materials for Oxygen Reduction Reaction Clarified Using Model Catalysts." *Science* 351: 361-5. https://doi.org/10.1126/science.aad0832.

[22] Dong, J.-C., Zhang, X.-G., Briega-Martos, V., Jin, X., Yang, J., Chen, S., Yang, Z.-L., Wu, D.-Y., Feliu, J. M., Williams, C. T., Tian, Z.-Q., and Li, J.-F. 2019. "In Situ Raman Spectroscopic Evidence for Oxygen Reduction Reaction Intermediates at Platinum Single-Crystal Surfaces." *Nat. Energy* 4: 60-7. https://doi.org/10.1038/s41560-018-0292-z.

[23] Jenkins, G. M., and Kawamura, K. 1971. "Structure of Glassy Carbon." *Nature* 231: 175-6. https://doi.org/10.1038/231175a0.

[24] Wu, Y., and Okajima, T., Ohsaka, T. 2017. "Lithium Intercalation into Graphene Ribbons of Glassy Carbon." *Int. J. Electrochem. Sci.* 12 (2): 1004-13. https://doi.org/10.20964/2017.02.48.

[25] Kim, H., Lee, K., Woo, S. I., and Jung, Y. 2011. "On the Mechanism of Enhanced Oxygen Reduction Reaction in Nitrogen-Doped Graphene Nanoribbons." *Phys. Chem. Chem. Phys*. 13: 17505-10. https://doi.org/10.1039/C1CP21665A.

[26] Wu, Y., Muthukrishnan, A., Nagata, S., and Nabae, Y. 2022. "Tafel Slope Analysis from Inherent Rate Constants for Oxygen Reduction Reaction over N-doped Carbon and Fe-N-doped Carbon Electrocatalysts." *Catal. Surv. Asia*. 27 (1): 1-11. https://doi.org/10.1007/s10563-022-09381-9.

[27] Seh, Z. W., Kibsgaard, J., Dickens, C. F., Chorkendorff, I., Nørskov, J. K., and Jaramillo, T. F. 2017. "Combining Theory and Experiment in Electrocatalysis: Insights into Materials Design." *Science* 355: eaad4998. https://doi.org/10.1126/science.aad4998.

[28] Zitolo, A., Goellner, V., Armel, V., Sougrati, M.-T., Mineva, T., Stievano, L., Fonda, E., and Jaouen, F. 2015. "Identification of Catalytic Sites for Oxygen Reduction in Iron- and Nitrogen-Doped Graphene Materials." *Nat. Mater.* 14: 937-42. https://doi.org/10.1038/nmat4367.

[29] Feng, W., Long, P., Feng, Y. Y., and Li, Y. 2016. "Two-Dimensional Fluorinated Graphene: Synthesis, Structures, Properties and Applications." *Advanced Science* 3 (7): 1500413. Accessed June 6, 2022. https://onlinelibrary.wiley.com/doi/10.1002/advs.201500413.

[30] Peera, S. G., Arunchander, A., and Sahu, A. K. 2016. "Platinum Nanoparticles Supported on Nitrogen and Fluorine Co-doped Graphite Nanofibers as an Excellent and Durable Oxygen Reduction Catalyst for Polymer Electrolyte Fuel Cells." *Carbon* 107: 667-79. https://doi.org/10.1016/j.carbon.2016.06.021.

[31] Peng, H., Liu, F., Qiao, X., Xiong, Z., Li, X., Shu, T., and Liao, S. 2015. "Nitrogen and Fluorine Co-doped Carbon Catalyst with High Oxygen Reduction Performance, Prepared by Pyrolyzing a Mixture of Melamine and PTFE." *Electrochimica Acta.* 182: 963-70. https://doi.org/10.1016/j.electacta.2015.10.012.

[32] Peera, S. G., Sahu, A. K., Arunchander, A., Bhat, S. D., Karthikeyan, J., and Murugan, P. 2015. "Nitrogen and Fluorine Co-doped Graphite Nanofibers as High Durable Oxygen Reduction Catalyst in Acidic Media for Polymer Electrolyte Fuel Cells." *Carbon* 93: 130-42. https://doi.org/10.1016/j.carbon.2015.05.002.